

## On the interplay between lateral interactions, hydrophobicity and acid strength on catalytic activity of nanoporous sulphonic acid silicas.

Jean-Philippe Dacquin,<sup>a</sup> Hannah E. Cross,<sup>b</sup> D. Robert Brown,<sup>b</sup> Tina Düren,<sup>c</sup> Jennifer Williams,<sup>c</sup> Adam F. Lee<sup>\*a</sup> and Karen Wilson<sup>\*a</sup>

### Electronic Supplementary Information

#### 1. Parent MCM Characterisation:

**Figure S1** shows calcined MCM-41 sample exhibits well defined peaks at 2.1, 3.8 and 4.4° that are typically ascribed to the (100), (110) and (200) planes for the hexagonal arrangement of mesoporous channels of MCM-41 materials. The N<sub>2</sub> isotherms, where the parallel adsorption/desorption branches can be distinguished, are of type IV which is typical for a MCM-41 structure. The ordered material is characterised by a narrow pore size distribution (2.5 nm pore size diameter) combined with a high specific surface area (1044 m<sup>2</sup>.g<sup>-1</sup>).

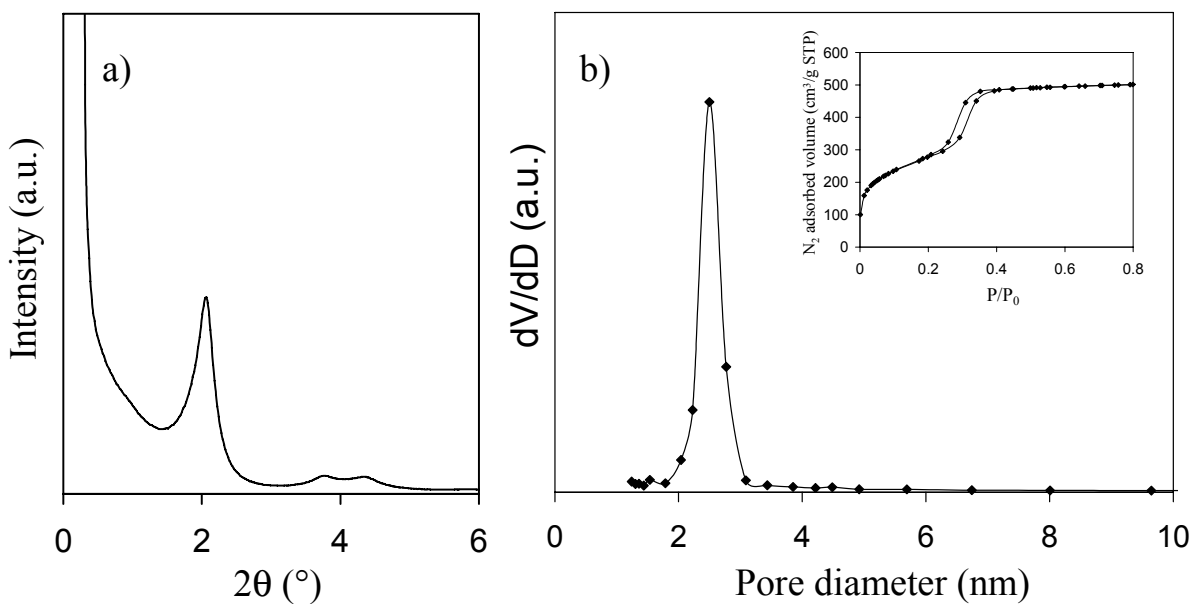


**Fig. S1:** Structural and textural properties of MCM-41 ; (a) X-ray diffraction pattern; (b) nitrogen adsorption-desorption isotherm and BJH pore diameter distribution.

TGA was used to assess the surface silanol density of the calcined MCM and thus grafting capacity of the silica. This was estimated by thermal analyses using TGA technique that were performed to probe the OH species coming from the surface silanols groups. As highlighted in **Figure S2**, the initial weight loss that occurs up to 120°C is due to desorption of physically adsorbed water isolated -OH are then lost >600 °C, corresponding to dehydroxylation reactions at the SiO<sub>2</sub> surface [1].

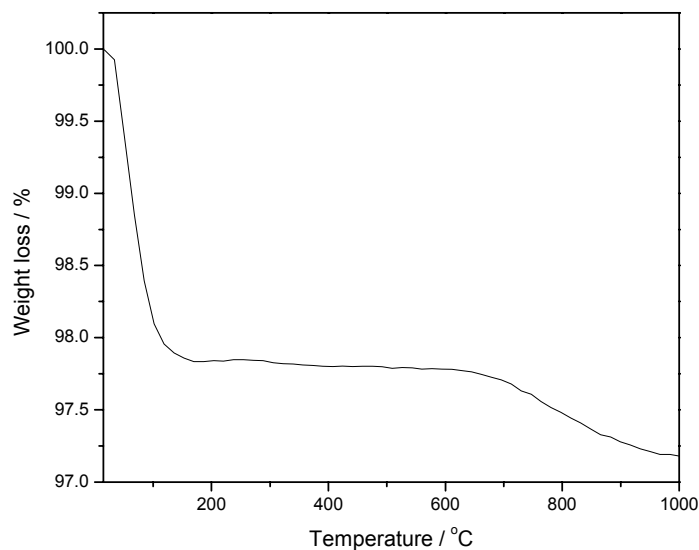


**Fig.S2:** Thermal analysis of the batch MCM-41 sample.

In order to check the structural integrity of MCM-41 materials post-functionalization, subsequent low angle XRD and N<sub>2</sub> porosimetry were performed on the oversaturated sulphonic acid silicas. As shown **figure S3** and **table S3**, MCM-SO<sub>3</sub>H<sub>ovs</sub> and MCM-Oc-SO<sub>3</sub>H<sub>ovs</sub> materials both exhibit long range ordering and high surface areas after the post-synthesis grafting process. A slight decrease of the mesopore size is observed and results from tethered sulphonic acid centers and steric hindrance of octyl chains but significant pore volumes remain after the loading process (**table S3**).

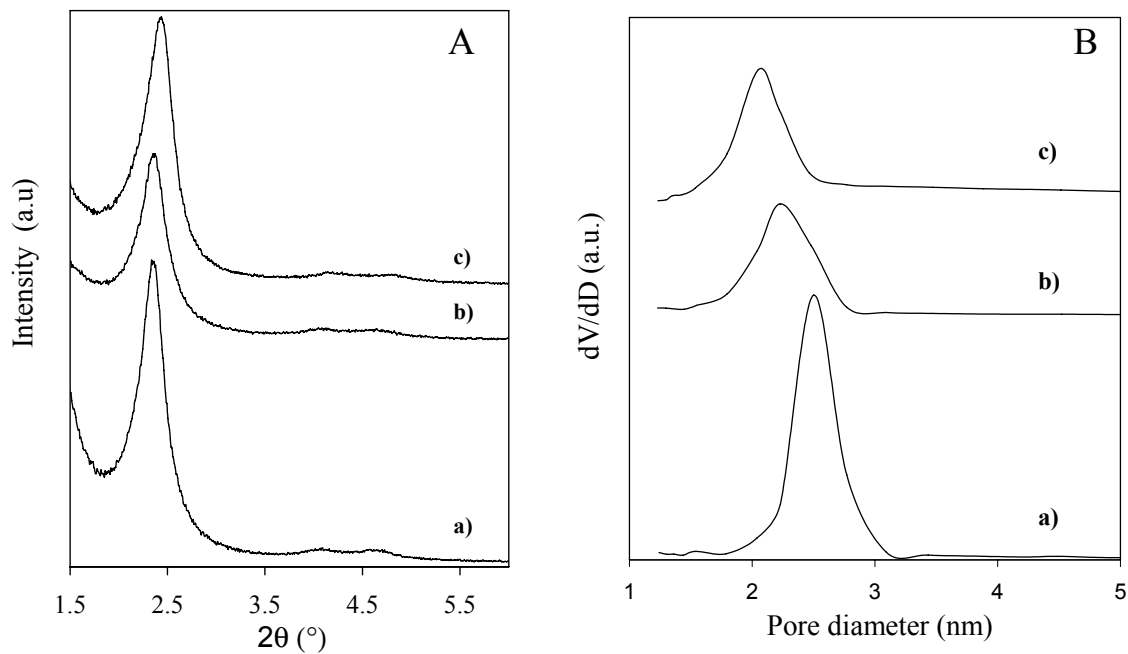


**Fig.S3:** Low angle XRD (A) and pore diameter distribution (B) of (a) MCM-41; (b) MCM-SO<sub>3</sub>H<sub>ovs</sub> and (c) MCM-Oc-SO<sub>3</sub>H<sub>ovs</sub> materials

**Table S1:** Textural properties of the fresh and sulphonic acid functionalized silicas.

Samples	Surface Area $\text{m}^2 \cdot \text{g}^{-1}$	Mesopore Volume $\text{cm}^3 \cdot \text{g}^{-1}$	BJH pore diameter nm
Fresh MCM-41	1044	0.98	2.49
MCM-SO <sub>3</sub> H <sub>ovs</sub>	747	0.66	2.25
MCM-SO <sub>3</sub> H <sub>100</sub>	800	/	/
MCM-SO <sub>3</sub> H <sub>75</sub>	875	/	/
MCM-SO <sub>3</sub> H <sub>50</sub>	950	/	/
MCM-SO <sub>3</sub> H <sub>25</sub>	992	0.74	2.43
MCM-Oc-SO <sub>3</sub> H <sub>ovs</sub>	942	0.85	2.05
MCM-Oc-SO <sub>3</sub> H <sub>100</sub>	920	/	/
MCM-Oc-SO <sub>3</sub> H <sub>50</sub>	870	/	/
MCM-Oc-H <sub>25</sub>	829	0.61	1.80

**Table S2a:** Bulk and surface compositions for MCM-SO<sub>3</sub>H samples

Samples	Bulk composition		Surface Composition		
	Bulk S content /mmol.g <sup>-1</sup>	Surface S content /mmol.g <sup>-1</sup>	S 2p / wt.%	C 1s / wt.%	Si 2p / wt.%
MCM-SO <sub>3</sub> H-ovs	0.58	0.28	0.96	5.96	33.39
MCM-SO <sub>3</sub> H-100	0.49	0.21	0.73	4.02	33.40
MCM-SO <sub>3</sub> H-75	0.27	0.16	0.49	3.10	30.98
MCM-SO <sub>3</sub> H-50	0.22	0.13	0.42	2.92	33.28
MCM-SO <sub>3</sub> H-25	0.15	0.09	0.30	2.54	31.02

**Table S2b:** Bulk and surface compositions for the MCM-Oc-SO<sub>3</sub>H series

Samples	Bulk composition		Surface Composition		
	Bulk S content /mmol.g <sup>-1</sup>	Surface S content /mmol.g <sup>-1</sup>	S 2p / wt.%	C 1s / wt.%	Si 2p / wt.%
MCM-Oc-SO <sub>3</sub> H-ovs	0.58	0.10	0.36	2.87	32.62
MCM-Oc-SO <sub>3</sub> H-100	0.52	0.09	0.32	3.37	31.94
MCM-Oc-SO <sub>3</sub> H-50	0.13	0.09	0.22	5.84	31.12
MCM-Oc-SO <sub>3</sub> H-25	0.07	0.07	0.15	8.32	32.46

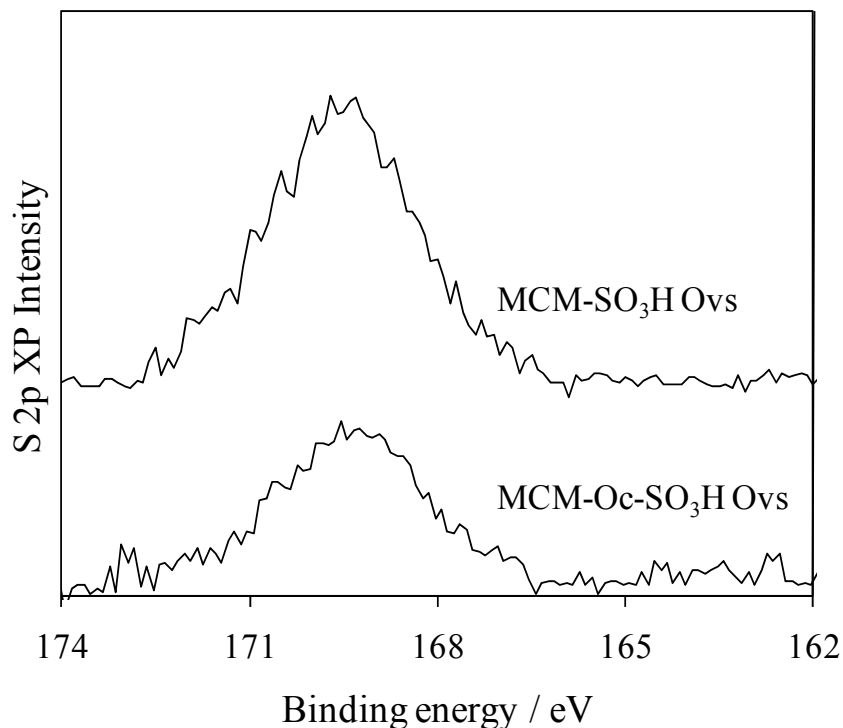


**Fig. S4:** S(2p) XPS spectra of (a) MCM-SO<sub>3</sub>H-ovs and (b) MCM-Oc-SO<sub>3</sub>H-ovs showing complete oxidation to sulphonic acid.



**2. Catalyst activity in butanol esterification:**

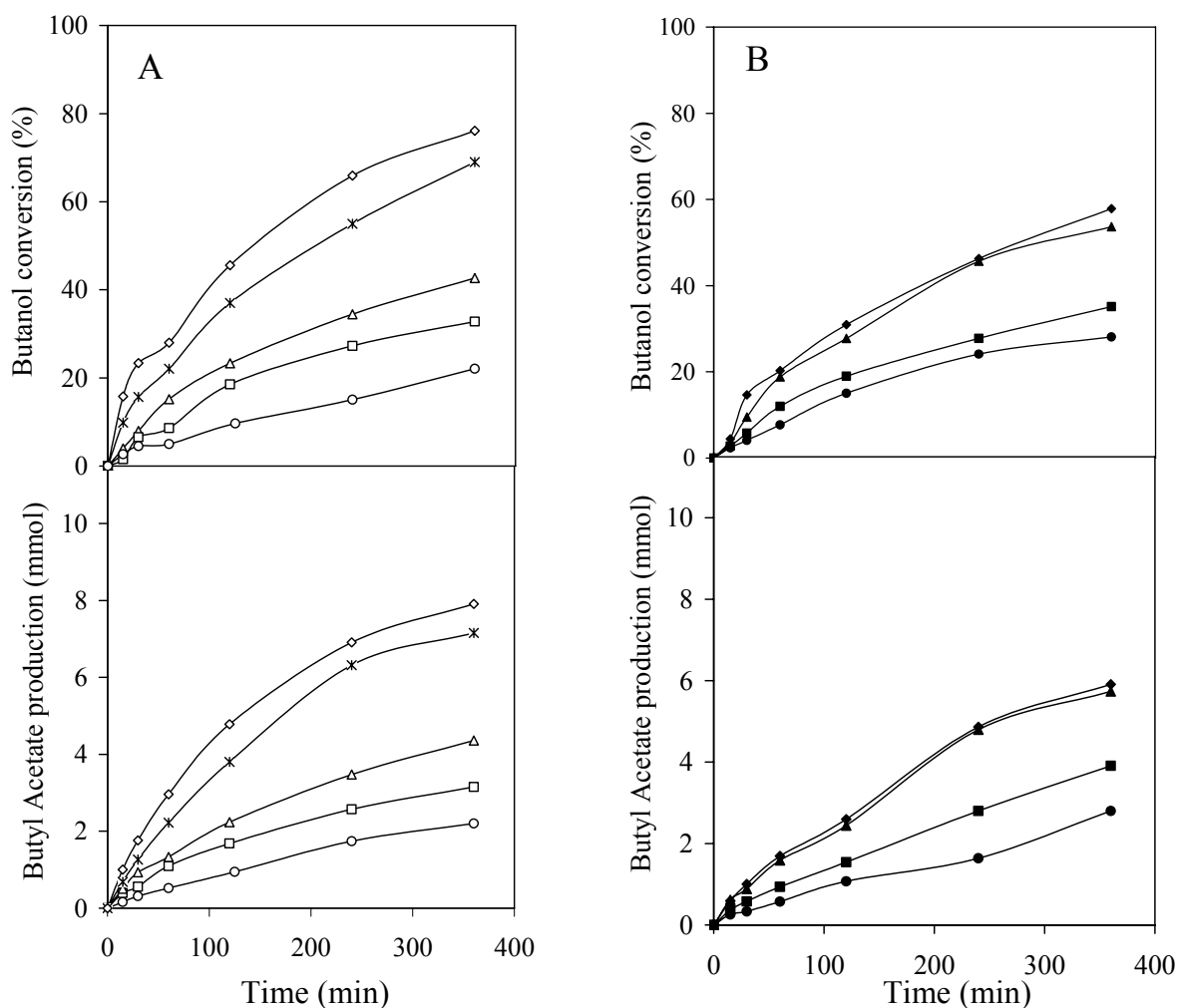


**Fig. S5:** Esterification reaction of butanol with acetic acid over sulphonic acid catalysts. A) MCM-SO<sub>3</sub>H series, (◊) MCM-SO<sub>3</sub>H ovs; (\*) MCM-SO<sub>3</sub>H-100, (Δ) MCM-SO<sub>3</sub>H-75, (□) MCM-SO<sub>3</sub>H-50, (○) MCM-SO<sub>3</sub>H-25; (B) MCM-Oc-SO<sub>3</sub>H series; (◆) MCM-Oc-SO<sub>3</sub>H-ovs , (▲) MCM-Oc-SO<sub>3</sub>H-100 , (■) MCM-SO<sub>3</sub>H-50, (●) MCM-Oc-SO<sub>3</sub>H-25

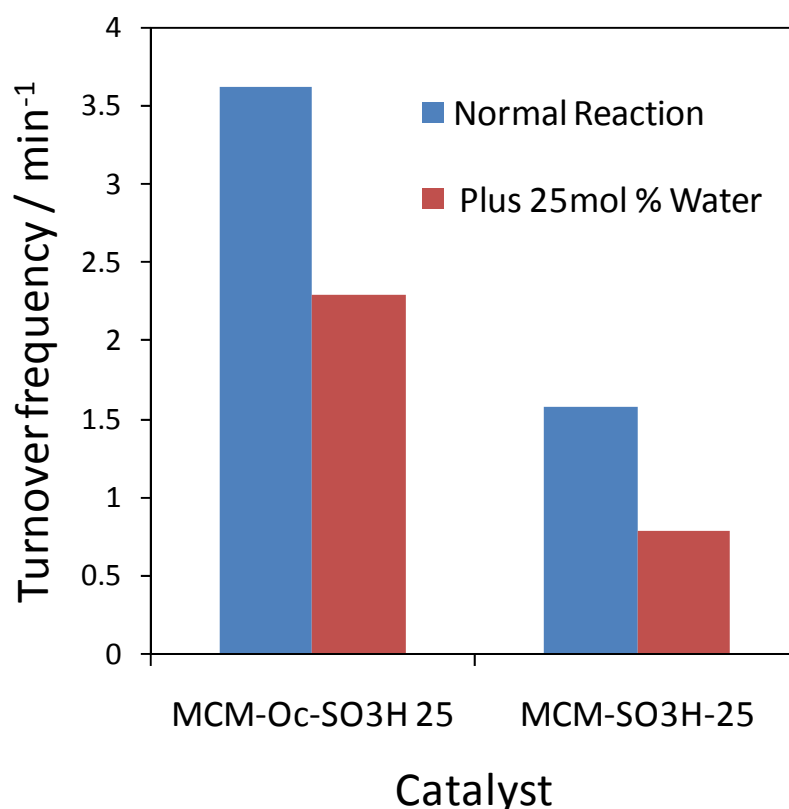


**Fig. S6:** Effect of H<sub>2</sub>O addition on TOF of MCM-Oct-SO<sub>3</sub>H-25 and MCM-SO<sub>3</sub>H-25 in esterification reaction of butanol with acetic acid.

### 3. Molecular Simulations:

To ensure that the MCM-41 pore model used in the simulation work was an accurate representation of the real material, the N<sub>2</sub> adsorption properties of the experimental and simulated pore at 77K were compared. See **Figure S7**.

The simulated isotherm was obtained using GCMC simulations<sup>2,3</sup> of N<sub>2</sub> adsorbed in the model pore. The model used for N<sub>2</sub> was obtained from Murthy<sup>4</sup>. The parameters for MCM-41 were the same as those used for the molecular dynamics simulations and are described below.

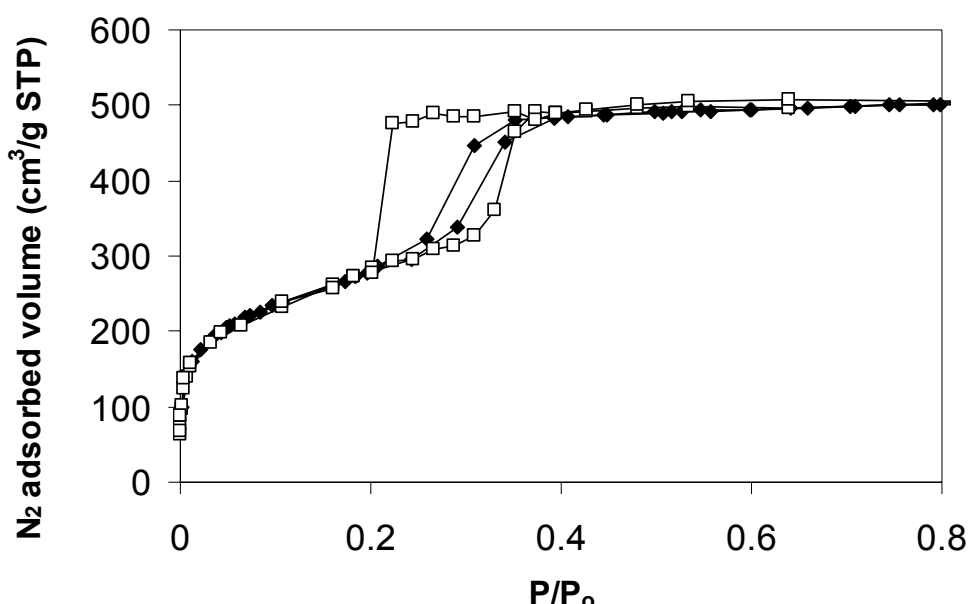


**Figure S7.** Adsorption isotherms of N<sub>2</sub> at 77K on unfunctionalised MCM-41 (◆) experimental isotherm (○) simulated isotherm.

Figure S5 shows that although the hysteresis is broader in the simulated isotherm than the experimental one, the general shape of the isotherm including the point of inflection is in very good agreement with the experimental data confirming that the simulated pore model is a reasonable representation of the real 2.5 nm MCM-41 material.

In order to express in a quantitative manner, the degree to which the surface group interacted with the pore wall, an angle  $\phi$  was defined as the angle between three vector points. Vector point 1 ( $x_1, y_1, z_1$ ) was defined as the coordinates of the silicon atom to which the C<sub>3</sub>H<sub>7</sub>SO<sub>3</sub>H group was anchored. Vector point 2 ( $x_2, y_2, z_2$ ) was defined as the coordinates of the sulphur group of the propylsulphonic acid. Vector point 3 (0, 0,  $z_1$ ) was defined as the centre of the

pore with the same z coordinate as the anchoring silicon atom. This is illustrated in **Figure S8a.**

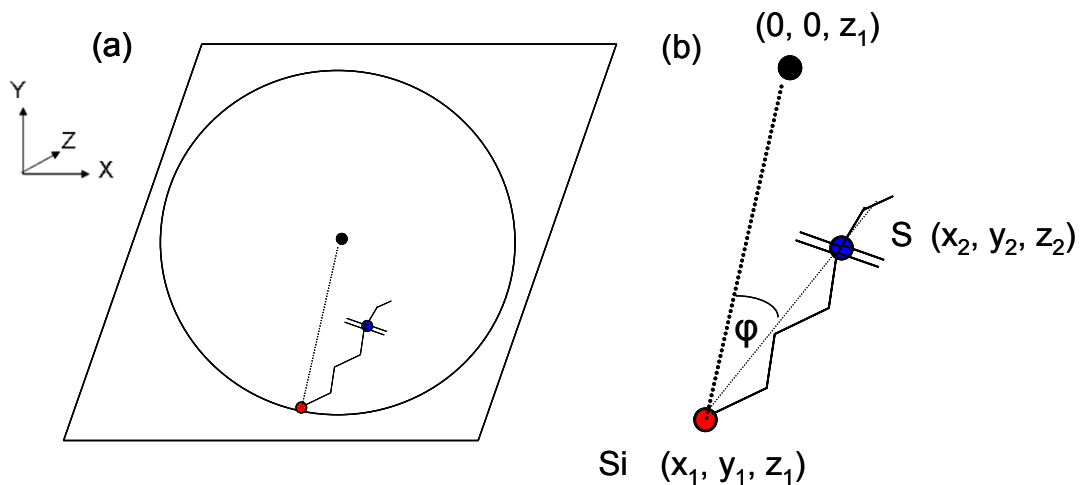


**Figure S8a.** The coordinates used to define  $\phi$ , used as a measure of the interaction of the  $\text{C}_3\text{H}_7\text{SO}_3\text{H}$  groups with the surface.  $\phi$  is the angle between the centre of the pore  $(0,0,z_1)$ , the anchoring Silicon atom  $(x_1,y_1,z_1)$  and the terminal Sulphur group  $(x_2,y_2,z_2)$ .

Angle  $\phi$  is therefore a measure of the orientation of the surface group with respect to the pore wall which in turn is determined by the extent of the interaction between the pore wall and the surface group. A group which shows little interaction with the pore wall (i.e. is oriented towards the pore centre) will have a small  $\phi$ . For a group which interacts strongly with the pore wall i.e. lies across the pore wall  $\phi$  will be large (see **Figure S8b**).

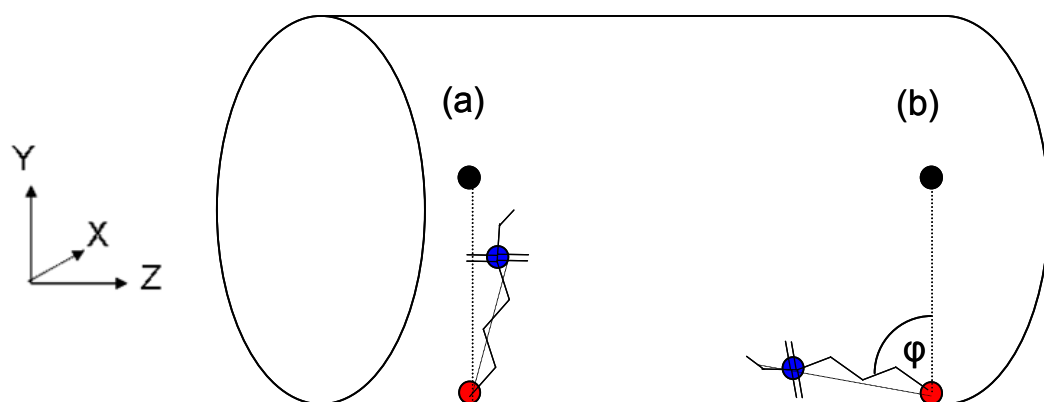


**Figure S8b.** The two extreme positions of the surface group (a) oriented perpendicular to the pore wall and making an angle  $\phi \approx 0^\circ$ . (b) lying along the pore wall with  $\phi \approx 90^\circ$ . The amorphous nature of the simulated silica pore wall which encompasses microcavities and recesses can give rise value of  $\phi$  greater than  $90^\circ$ .

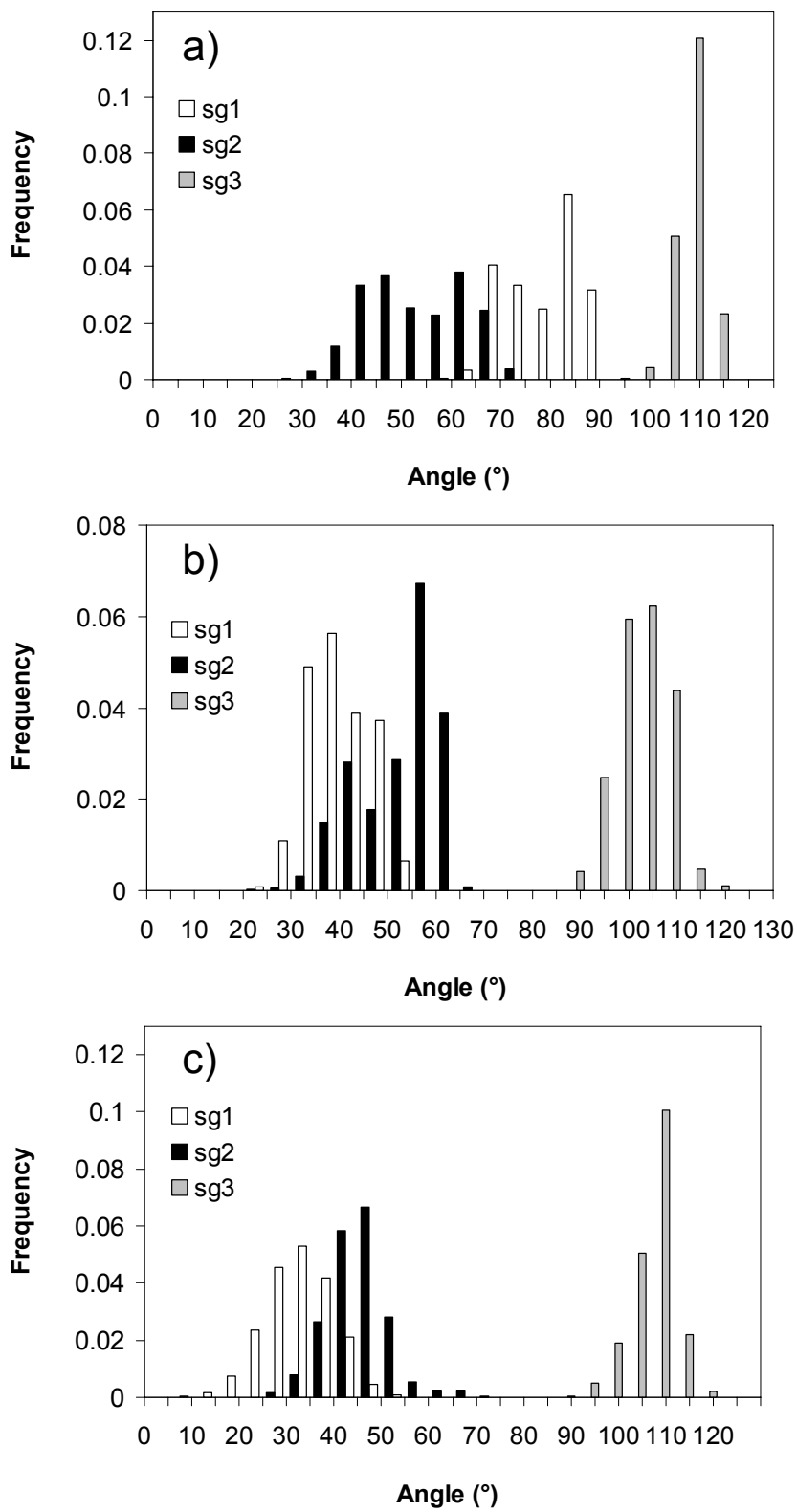


**Figure S9.** Distribution of  $\phi$  for the three different surface groups of (a) 0.15 mmol/g MCM-SO<sub>3</sub>H, (b) 0.58 mmol/g MCM-SO<sub>3</sub>H and (c) 0.15mmolg SO<sub>3</sub>H/0.43mmol/g Octyl functionalized MCM-Oc-MCM-41. Surface group (sg) 1 and sg2 are in close proximity of each other, sg3 is isolated as illustrated in Scheme 3 of main article.

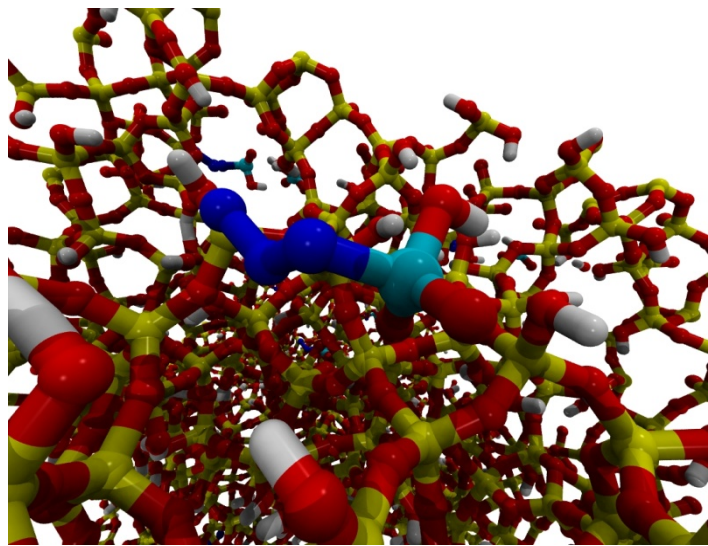


**Figure S10:** Surface group 3 on 0.15mmolg<sup>-1</sup> MCM-SO<sub>3</sub>H interacting with a surface hydroxyl

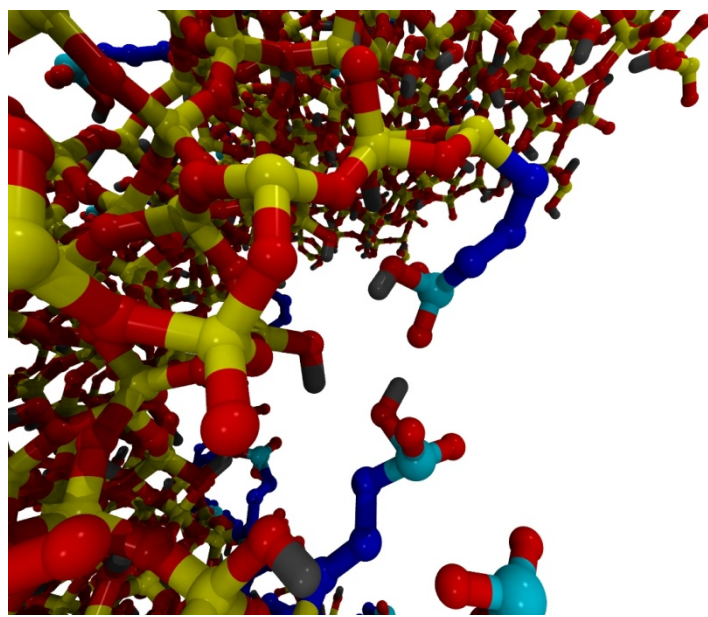


**Figure S11:** Surface group 1 and 2 on 0.58mmolg<sup>-1</sup> MCM-SO<sub>3</sub>H interacting with each other.

**Parameters for Simulation:**

All movies are available at: <http://www.see.ed.ac.uk/~tduren/Movies/>

This section provides details of the potential models used in the molecular dynamics simulations presented in the main article.

The MCM-41 consisted of tetrahedrally coordinated atoms of silicon, oxygens bonded to Silicon (bO) and oxygens terminating in a surface hydroxyl group (nbO). The potential parameters for the Si, bO, nbO and H were taken from published data.<sup>5</sup> Here and in the main article we refer to our MCM-41 model as having a pore diameter of 38 Å. It should be noted, however, that as the pores walls of MCM-41 are amorphous, there is no clearly defined pore diameter. The pore diameters used in this paper were calculated from the accessible pore volume which was estimated by simulating the adsorption of helium at 0.3 bar and 293K<sup>6</sup>.

For the surface groups, CH<sub>2</sub> and CH<sub>3</sub> groups forming alkyl chains were represented by one pseudo atom each but all other atoms are modelled explicitly. Thus the propyl sulphonic acid surface groups C<sub>3</sub>H<sub>7</sub>SO<sub>3</sub>H consisted of 8 sites, three CH<sub>2</sub> sites (CH<sub>1</sub>, CH<sub>2</sub>, CH<sub>3</sub>), a Sulphur site (S), two doubly bonded oxygen sites (OD1 and OD2) and hydroxyl group consisting of an oxygen (OH\_S) and a hydrogen site (H\_S). The octyl group consisted of 8 sites, seven united atom CH<sub>2</sub> sites and a terminal CH<sub>3</sub> site. The interaction between surface groups and the surface group and pore wall is assumed to be strictly physical. The partial charges on the atoms of these molecules are represented by effective point charges with the functionalized MCM-41 molecule being overall electrostatically neutral.

The MCM-41 framework was kept frozen during the simulation but the propylsulphonic acid, octyl and hydroxyl groups were fully flexible. A united-atom model was used for the octyl and propyl chain of the sulphonic acid groups.

Partial charges and non bonded parameters for the organic chain molecules were adopted from the optimized potentials for liquid simulations (OPLS) force field.<sup>7,8</sup>. In the case of the sulphonic acid groups, these were generated using Boss v.4.8.<sup>9</sup> Bond stretching, angle bending and torsional potential parameters were generated from the gromacs 87 force-field<sup>10</sup> using the PRODRG server.<sup>11</sup>

The force field includes bending, stretching and torsional terms, Lennard-Jones (L-J) interactions, and Coulomb electrostatics. The bond stretching between two covalently bonded atoms was represented by a harmonic potential of the form:

$$U = \frac{1}{2}k(r - r_o)^2$$

Angles were modelled by a harmonic potential of the form:

$$U = \frac{1}{2}k(\theta - \theta_o)^2$$

Improper dihedrals were represented by the harmonic potential of the form:

$$U = \frac{1}{2}k(\xi - \xi_o)^2$$

Proper dihedral interactions were modelled using the periodic dihedral:

$$U(\phi_{ijkl}) = k_\phi(1 + \cos(n\phi - \phi_s))$$

The inter-molecular potential is the sum of a Lennard-Jones (L-J) term and a Coulombic term:

$$U_{ij} = 4\epsilon_{ij} \left[ \left( \frac{\sigma_{ij}}{r_{ij}} \right)^{12} - \left( \frac{\sigma_{ij}}{r_{ij}} \right)^6 \right] + f \frac{q_i q_j}{r_{ij}}$$

In the above equations,  $U$  is the potential energy,  $\theta$  is the instantaneous bond angle,  $\theta_0$  is the equilibrium bond angle,  $k$  is a harmonic force constant,  $\varphi$  is the instantaneous dihedral angle,  $\sigma$  is the L-J site diameter,  $\epsilon$  is the L-J well depth,  $q$  is the site partial charge,  $f$  is a constant (accounting for the vacuum permittivity) with the value of 138.935485 and  $r_{ij}$  is the distance between sites  $i$  and  $j$ . Long-range electrostatic interactions were treated using the particle-mesh Ewald method.<sup>12</sup> All Lennard Jones interactions were truncated beyond 9.5 Å. The following tables present the intra- and inter-molecular potential parameters used in the MD simulations.

**Table S3 – Lennard-Jones parameters, point charges and atomic masses.**

Site	$\sigma$ (nm)	E (kJ mol <sup>-1</sup> )	q (a.u.)	Mass (a.u.)
Si	0.0	0.0	1.2805	28.086
bO	0.2708	1.5381	-0.6405	15.9994
nbO	0.30	1.5381	-0.5261	15.9994
H	0.0	0.0	0.2060	1.00797
CH1	0.3905	0.493712	-0.2795	14.0271
CH2	0.3905	0.493712	0.0682	14.0271
CH3	0.3905	0.493712	-0.1655	14.0271
S	0.355	1.046	1.3901	32.066
OD1, OD2	0.296	0.71128	-0.5667	15.9994
OH_S	0.312	0.71128	-0.5667	15.9994
H_S	0.0	0.0	0.5072	1.00797
OC1	0.3905	0.493712	-0.22012	14.02709
OC2	0.3905	0.493712	-0.1	14.02709
OC3-OC7	0.3905	0.493712	0.0	14.02709
OC8	0.375	0.493712	0.0	15.03452

**Table S4 – Bond lengths and stretching constants.**

Bond	Length (nm)	K (kJ mol nm <sup>-2</sup> )
SI – bO	0.161	251040
SI – nbO	0.16	251040
nbO – H	0.0945	313800
SI – CH1	0.1865	334720
CH1 – CH2	0.1529	334720
CH2 – CH3	0.1529	334720
S – CH3	0.177	376560
OH_S – S	0.167	334720
OD1 – S	0.144	376560
OD2 – S	0.144	376560
OH_S – H_SP	0.09451	313800
SI – OC1	0.188	334720
OC1 – OC2	0.1526	334720
OC2 – OC3	0.1526	334720
OC3 – OC4	0.1526	334720
OC4 – OC5	0.1526	334720
OC5 – OC6	0.1526	334720
OC6 – OC7	0.1526	334720
OC7 – OC8	0.1526	334720

**Table S5 – Bond angles and harmonic force constants.**

Angle	$\theta_0$ (degrees)	K (kJ mol <sup>-1</sup> rad <sup>-2</sup> )
Si -bO -Si	155	397.48
nbO - SI -nbO	109.5	397.48
bO - SI - nbO	109.5	397.48
bO - SI -bO	109.5	397.49

SI - nbO - H	109.5	397.48
bO - SI - CH1	109.5	397.48
nbO - Si - CH1	109.5	397.48
SI - CH1 - CH2	112	519.6
CH1 - CH2 - CH3	112	519.6
CH2 - CH3 - S	108.6	418.4
CH3 - S - OH	96.4	627.6
CH3 - S - OD1	108.9	619.2
C3 - S - OD2	108.9	619.2
OH_S - S - OD1	108.7	619.2
OH_S - S - OD2	108.7	619.2
OD1 - S - OD2	119	870.2
S - OH_S - H_SP	110	619.2
O - SI - OC1	109.5	397.48
OH - SI - OC1	109.5	397.48
SI - OC1 - OC2	111	460.2
OC1 - OC2 - OC3	111	460.2
OC2 - OC3 - OC4	111	460.2
OC3 - OC4 - OC5	111	460.2
OC4 - OC5 - OC6	111	460.2
OC5 - OC6 - OC7	111	460.2
OC6 - OC7 - OC8	111	460.2

**Table S6 – Dihedral potential parameters.**

Dihedral	$\Phi$ (deg)	$k_\phi$ (kJ mol <sup>-1</sup> )
bO - SI - bO - SI	3.765	3
bO - SI - nbO - H	3.766	3
nbO - SI - nbO - H	3.766	3
nbO - Si - bO - SI	3.766	3
Si - bO - SI - CH1	3.8	3
CH2 - CH1 - SI - bO	5.9	3
CH2 - CH1 - SI - nbO	1.3	3
SI - CH1 - CH2 - CH3	5.9	3
CH1 - CH2 - CH3 - S	5.9	3
OD1 - S - CH3 - CH2	2.9	3
CH3 - S - OH_S - H_S	2.9	3
SI - bO - SI - OC1	3.8	3
SI - OC1 - OC2 - OC3	5.9	3
OC2 - OC1 - SI - bO	5.9	3
OC2 - OC1 - SI - nbO	1.3	3
OC1 - OC2 - OC3 - OC4	5.9	3
OC2 - OC3 - OC4 - OC5	5.9	3
OC3 - OC4 - OC5 - OC6	5.9	3
OC4 - OC5 - OC6 - OC7	5.9	3
OC5 - OC6 - OC7 - OC8	5.9	3

**Table S7 – Improper Dihedral potential parameters.**

Improper Dihedral	$\xi_0$	$k_\xi$ (kJ mol <sup>-1</sup> rad <sup>-2</sup> )
S - CH3 - OD1 - OD2	35.3	836.8

**References:**

- 
- 1 C. Zhang, W. Zhou, and S. Liu, *J. Phys. Chem. B* 2005, **109**, 24319.
  - 2 C. Schumacher, J. Gonzalez, M. Perez-Mendoza, P. Wright and N. Seaton, *N. Ind. Eng. Chem. Res.* 2006, **45**, 5586.
  - 3 C. Schumacher J. Gonzalez, M. Perez-Mendoza, P. Wright and N. Seaton, *N. Stud. Surf. Sci. Catal.* 2004, **154**, 386.
  - 4 C. Murthy, K. Singer, M. Klein and I. McDonald, *Mol. Phys.* 1980, **41**, 1387.
  - 5 A. Brodka, A and T. Zerda, *J. Chem. Phys.* 1996, **104**, 6319.
  - 6 O. Talu and A. Myers, *Aiche Journal* 2001, **47**, 1160.
  - 7 W. Jorgensen, J. Madura and C. Swenson, *J. Am. Chem. Soc.* 1984, **106**, 6638.
  - 8 W. Jorgensen, D. Maxwell and J. TiradoRives *J. Am. Chem. Soc.* 1996, **118**, 11225.
  - 9 W. Jorgensen and J. Tirado-Rives, *J. Comput. Chem.* 2005, **26**, 1689.
  10. van Gunsteren and Berendsen, Groningen Molecular Simulation (GROMOS) Library Manual, BIOMOS b.v., Groningen, 1987.
  11. W. Schuettelkopf, D. van Aalten, *Acta Crystallogr.* 2004, **D60**, 1355.
  12. U. Essman, L. Perela, M. Berkowitz, T. Darden, H. Lee, L. Pedersen, *J. Chem. Phys.* 1995, **103**, 8577.